Journal of the European Ceramic Society 23 (2003) 455–468

www.elsevier.com/locate/jeurceramsoc

Thermal shock resistance and thermal-mechanical processing of sapphire

A.G. Lanin*, E.L. Muravin, V.P. Popov, V.N. Turchin

Scientific Research Institute of SIA "LUCH", Podolsk, 142100, Russia

Received 15 November 2001; received in revised form 6 March 2002; accepted 11 April 2002

Abstract

The finite elements method was applied to calculate transient thermal stresses in sapphire with taking into account the crystal's anisotropy, scale factor, temperature function of heat transfer and other properties. The sapphire fracture behaviour as compared to ceramic polycrystalline materials under heat load, differs due to two factors: (a) twinning type strain at rather low test temperatures <200 °C and (b) fracture toughness anisotropy. The cracking behaviour and thermal shock resistance (TSR) of the crystal against its dimensions, orientation and the heat load type was explained using the force fracture mechanics and the twinning and cracking features in the tensile and compressive stress fields. The influence of residual stresses after stress relaxation was studied. A possibility to increase the strength by 2–3 times and TSR of sapphire using a thermomechanical process was shown. This enables thermal stress generation under high-rate heatup to 1500–2000 °C, thus lowering the stress concentration on defects through local stress relaxation. © 2002 Elsevier Science Ltd. All rights reserved.

Keywords: Al_2O_3; Fracture; Heat treatment; Modelling; Sapphire; Thermal shock resistance

1. Introduction

Aluminum oxide as polycrystal and single crystal (sapphire), has found a use in recent years in structural applications, where a resistance to high heat loads and temperature drops (e.g. parts for space plants) are of great importance. To choose materials for these applications, important is such a parameter as thermal shock resistance (TSR). Unlike polycrystal Al_2O_3, whose TSR was studied in many works (e.g. Refs. 1–3), any data on the single crystal sapphire TSR is almost absent in related literature, though sapphire has been widely in practice to the moment.[4] The TSR and failure is influenced by the sapphire crystal orientation, stress–strain condition, defects on its surface and in volume, that has not yet been studied. Besides, available data on the strength and fracture of differently oriented sapphire crystals under mechanical load[5] indicate, that also thermal load may have a significant effects on the above. So, a research on the TSR of sapphire under various conditions is of great interest, also because this reveals a possibility to strengthen sapphire products (e.g. through a thermomechanical process). To quantify the TSR, a heat-stress calculation procedure taking into consideration the crystal anisotropy and non-linear boundary conditions of heat exchange was developed.

2. Experimental procedure

2.1. Sample preparation

Most sapphire crystals for experiments were grown in Research Institute of SIA "LUCH" by a method of directional crystallization (Stepanov's method)[6] through extraction of a specified profile crystal from a melt with a seed having a given crystallographic orientation. The sapphire blanks were obtained as rods 4–5 mm in diameter and 350 mm long, as pipes 16 mm OD, 8.0 mm ID and 100–120 mm long and as plates 40 mm wide, 4 mm thick and up to 200 mm long. The rods' and tubes' growth axes were oriented $<0001>$, $<011\ \bar{2}>$ within 2–4° and $\{11\ \bar{2}0\}$- plates were $<10\ \bar{1}0>$-oriented.

The extraction rate was 1 mm/min. Maximum 0.7 mm blocks were observed on separate sites of the crystal.

* Corresponding author.
E-mail address: iifedik@podolsk.ru (A.G. Lanin).

0955-2219/02/$ - see front matter © 2002 Elsevier Science Ltd. All rights reserved.
PII: S0955-2219(02)00093-6

Crystals with disorientation of the blocks more than 3° were rejected. The average density of dislocations on the growth surface was 10^5 cm^{-2}. The blanks in a batch were somewhat different in porosity. A noticeable non-uniformly distributed porosity was observed in rods batches IV and V. 1–3 μm pores were concentrated in the middle of the rods from batch VI with a maximum pore density 10^4 mm^{-2}. A grid of pores was observed on the surface of the samples (batch VII). The porosity was mainly distributed in on the outside of plates and tubes, which was removed by machining the specimens. Cutting of blanks was conducted by a metal-bound diamond wheels with a 125–100 μm diamond grain. The surfaces of cylinder bars were ground in a water-oil emulsion by organic bound diamond wheels (AC6) with a 63–80 μm grain.

The sapphire disks 20–30 mm in diameter were prepared from the plates, cut to square pieces and then glued together. Such a glued unit was machined in a circular grinder by diamond wheels (AC6). The front face of disks was subjected to successive double side polishing to remove the surface porosity by diamond wheels 125/100, 40/28 and 28/20. The edges of disk were 45° chamfered by a free abrasive 40/28 μm. The front face was finished on a 10/7 μm diamond paste to remove 20–30 μm of damaged layersμ and then chemically polished on chamois with selicole. The final roughness of the surface was no more than $R_z = 0.05$ μm. The outside, inside and end faces of the tube samples were polished in similar modes.

2.2. Test methods

The TSR of sapphire was measured using non-stationary methods[7] by heating the lateral area of cold specimens in a bath with melted tin of a known temperature, or by quenching specimens, heated up to a preset temperature in a water bath. The samples were quenched as a rule horizontally. The procedure of water quenching of the lateral area of the disk specimen, having thermally insulated end faces, consists in a serial increase of the specimen temperature, through every 10–15 °C, until first appearance of cracks (readily visible without any penetrant) at reached temperature difference ΔT between the heated sample and water bath. In heating test, the melted tin temperature also increased every 20–30 °C and the difference ΔT, initiating the fracture, was registered using an acoustic sensor operating in the frequency range 1–20 kHz.

Thermal-mechanical processing and TSR measurement under single and cyclical thermal loading at elevated temperatures were conducted in our high-frequency installation (Fig. 1a).[8] A specimen (1) is heated in a hot chamber (2) in an inert medium or in vacuum up to

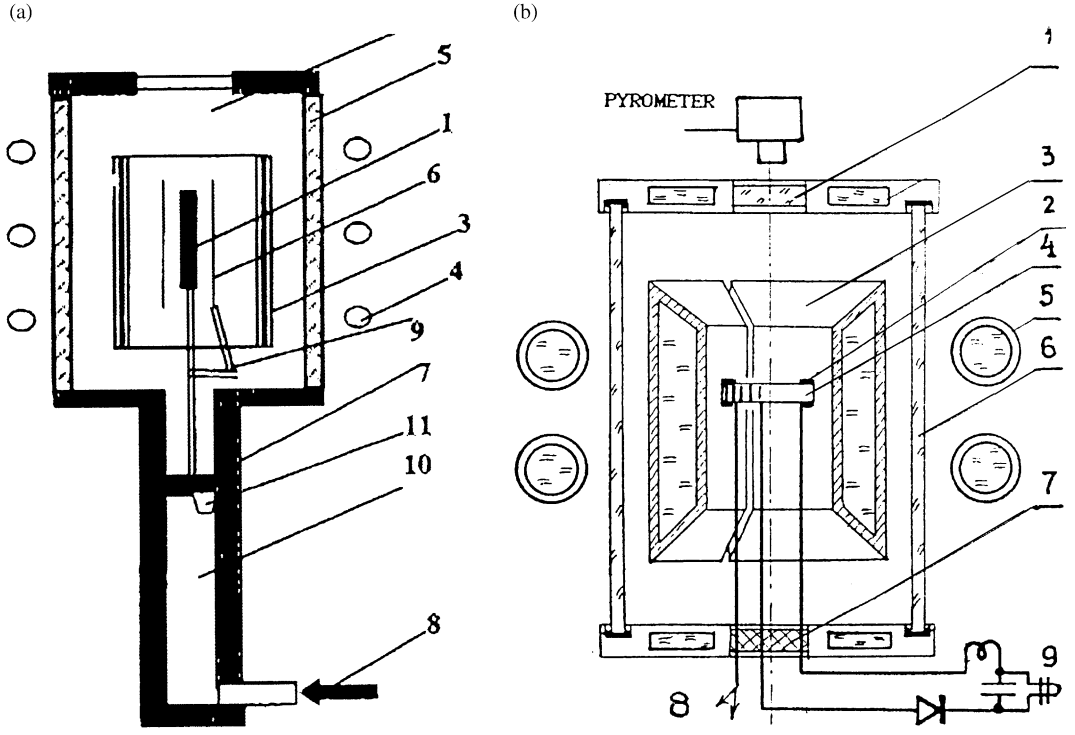

Fig. 1. Schematic diagrams of induction heating unit I (a) and II (b) for measurement of TSR at elevated temperatures.

2000 °C. The heater (3) is a hollow molybdenum cylinder placed inside an inductor (4). The heater is shielded from surroundings by water-cooled double quartz tubes (5). To create a uniform temperature field on the length of the heater, its end faces are protected by molybdenum screens. The temperature of the heater is monitored by an optical pyrometer. After the heater has reached the desired temperature, the specimen [protected on the side face by a shield (6)] is transferred pneumatically from the cold to hot chamber by a pusher (7), fed with compressed gas (8) via its lower side. After the specimen has been positioned in the middle of the heater, a screen pawl (9) is released and the screen drops by gravity, exposing the side face of the specimen. After a predetermined short exposure and relaxation of local thermal stresses, the specimen is transferred into the cold chamber (10). If the thermal stresses exceed the ultimate strength, the specimen fails, thus enabling determination of the TSR at a high temperature. In this event, the instant of the specimen fracture is fixed by a piezoelectric sensor (11), connected to the specimen through a sound guide; the signal from the sensor is transmitted through an amplifier to a recording oscillograph, which responds automatically after the screen drop.

A possibility for thermal stress to relax at a higher temperature and to determine the influence of the residual stresses on TSR was studied using a modified induction installation II[9] (Fig. 1b) with disks in an inert medium or directly in air. A disk (4) coated by thin-layer chromium, about 0.2 μm thick is placed on three insulated needles (7) within an induction coil (5) with a water-cooled copper concentrator (3), amplifying the magnetic field. The concentrator with a slanting cut serves also as a thermal screen, which allows the chamber (6) to be made of quartz. Both sides of the disk are covered at its periphery by rings (2) of an electrical conducting material (graphite). Under power supply to the induction heater, the rings and hence the specimen's peripheral area is heated up. Due to heat emission by radiation from the specimen's end parts, a temperature drop occurs in the disk. The temperature field along the disk's radius is measured by a thermocouple (8) or by an unsteady-state pyrometer through window (1). The TSR is estimated by the value of temperature drop ΔT between the specimen disk's centre and edge, sufficient to initiate the disk fracture at a known power. The fracture moment is defined by the registered break of an electric circuit (9) between three needles (7) supporting the specimenμ.

The three point bending strength σ of cylindrical specimens of diameter d tested on a device with a base l (here 20 mm) was calculated on the-load P from the ratio $\sigma = 8dl/\pi d^3$. Correction was made for the actual abscissa if fracture does not occur at l/2. The tests from 20 to 1800 °C were done in a testing machine with a tungsten heater and a 2500 mN load cell. The tensile strength of hollow cylinder was determined by internal pressure P_i tests from the ratio $\sigma_\theta = P_i\ (1+K^2)/(1-K^2)$, where σ_θ is the tangential stress on the internal surface, $K = d_i/d_o$ is the ratio of internal d_i to outer d_o diameter.[21] The fracture toughness was evaluated by indentation of a diamond Vickers pyramid under a 5 N load from the ratio $K_{1c} = 0.0726\ P\ c^{-3/2}$,,[21] where P is the load on the indentor; c is the radius of a hemi-disk crack.

The crystallographic orientation of the specimens was measured using a Dron-3 X-ray machine. The behaviour of cracks and twins was studied by microscopy under transmittance and reflection. The fracture surfaces were examined both by optical and scanning electron microscopy. The stresses after diamond processing of the sapphire surface were evaluated on the copper radiation line (half an X-beam is diffracted from a 8 mm depth). The lines were recorded in a 2θ scanning mode. The integral width of (1120) line was conditionally measured from the relation between the area under the curve K_α–doublet (till its coincidence with the background) and the line peak height. The measurements were conducted repeatedly to avoid a block structure effect; the received data were averaged.

2.3. Computational techniques for thermal stresses in isotropic and anisotropic bodies

The TSR of brittle ceramics is characterized usually by a critical temperature difference ΔT (between sample surface and quenching media) and by a value of stress σ responsible for fracture:[7]

$$\sigma = \alpha E \Delta T(\beta)/(1-\mu),$$

where E is the Young's modulus, α is the coefficient of linear heat expansion μ is the Poisson's constant. and the Biot number, $\beta = ah/\lambda$, where a is characteristic size, h is a heat transfer coefficient, λ is the materal's thermal conductivity. The coefficients of the heat transfer in water at 20 °C (Fig. 2a)[10] and in melted tin (Fig. 2b)[11] are determined experimentally. Determination of TSR (fracture stresses) are made by numerical methods on the basis of the quasi-static theory of thermal elasticity.[15] The non-linear boundary condition of the heat exchange and the temperature dependence of materials properties are taken into account. A disregard of these factors gives rise to errors in the calculation of thermal stresses, up to 20–50%.[12–14]

The temperature stresses at high-temperature heating are calculated from the heat flow value q facing the surface, which is, in turn, determined computationally from the value of reduced emissivity ε_r[16] or experimentally in a steady-state run,[17] by measuring the temperature as a function of time at a single point of a specimen[8] with a known value of its volumetric thermal capacity C_γ.

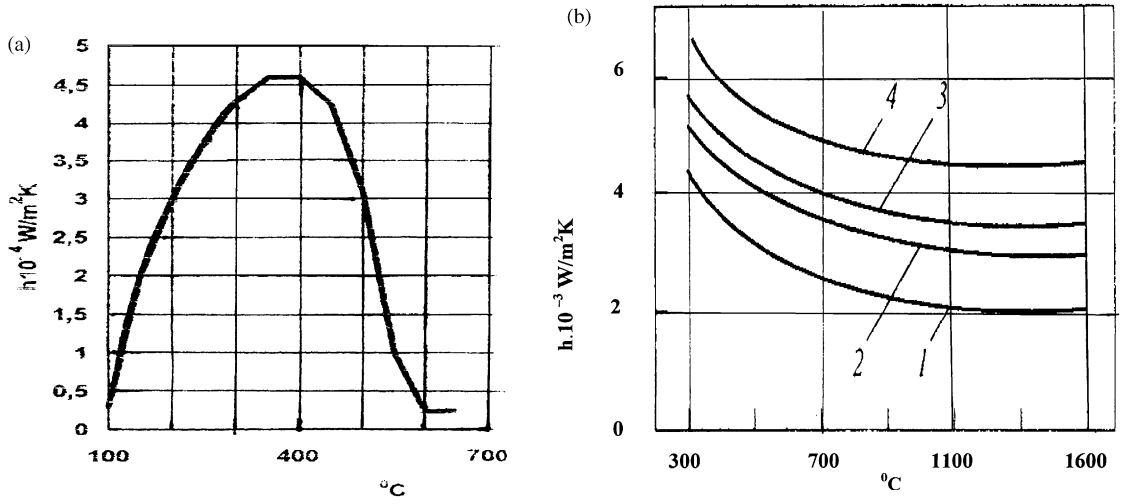

Fig. 2. Heat transfer coefficient of cylindrical specimen quenched in water (a) and of cylindrical specimens (with the wall thickness B and thermal conductivity λ) heated in molten tin (b) as a function of temperature. 1–4 refer to B/λ(m^2 K/w) 8×10^{-4}, 4×10^{-4}, 3×10^{-4}, 1.5×10^{-4} respectively.

Distribution of thermal stresses in the disk and cylindrical specimens of sapphire considering the anisotropy and temperature dependence of properties and coefficient of thermal emission was found by the finite elements method (FEM) using an ANSYS program complex.[18] Successive solution of unsteady non-linear problems of the thermal conductivity and the thermal elasticity in a spatial and axi-symmetrical statement should be done. The 2D meshing for axe-symmetrical and the 3D meshing for spatial state were used. The mesh division was performed with four-node rectangular elements for axial symmetry and with 20 nodes for spatial state. The number of node points and elements was dependent on the sample size. For example, the number of elements on radius, thickness, half circumference lay in the ratio of 8:5:12 for half disk 10 mm in diameter, 2.5 mm thick; on the whole were available 480 elements and 2491 nodes. The 2D FEM modelling of cylinder 3mm in diameter, 20 mm length had 1200 elements and 1281 nodes. The meshes were refined near the radial free surfaces.

As far as we know, a calculation of thermal stresses in sapphire, taking into account the anisotropy of properties and the non-linear heat exchange condition to determine the TSR, have not been made previously. Known only are methods to calculate thermal stresses in sapphire blanks grown from melts under axial temperature gradient[19,20] with the aim to optimise the growth parameters and decrease the dangerous residual stresses in the crystal.

The properties of (0001) oriented sapphire are presented in Table 1 across and along the C axis.

Solution of a thermal elasticity problem has a number of features. The first is essential nonlinearity of physical-mechanical properties of the material and change in the boundary conditions during the solving of the problem, especially sharp change (more than by one order) takes place under cooling a sample in water. Table 2 shows

Table 1
Properties of sapphire and polycrystyline Al_2O_3 versus temperature

Property	Orientation	Temperature, K			
		300	500	700	900
Thermal conductivity	∥	25	17.5	–	–
λ (W/mK)	⊥	–	–	–	–
	Polycrystal	23	15.5	8.6	8.5
Linear coefficient of thermal	∥	7.10	–	7.96	8.23
expansion, α (10^6 K^{-1})	⊥	5.50	–	6.60	7.22
	Polycrystal	6.30	–	7.45	7.74
Young's modulus E (GPa)	∥	460	–	–	–
	⊥	420	–	403	387
	Polycrystal	395	–	385	362

the influence of two parameters (heat conductivity λ and heat-transfer factor h) on the peak major stress σ_1 and time to reach it, for disks, (0001) oriented, cooled in water. The last line of Table 2 gives the solution for the non-linear problem statement.

The second feature is the anisotropy and scale factor. The (0001) oriented disks are transversally isotropic, disks with changed orientation possess properties of general anisotropy. Under a finite-elements simulation, a transition from the transversal isotropy to general anisotropy is derived automatically, if the C axis of the developed model is resolved in the main system of coordinates to which preset physical–mechanical properties of a transversally isotropic body are fixed. The character of the solution is changes, too. The solution is axi-symmetrical for disks with (0001) orientation and the problem may be solved for a two-dimensional (axi-symmetrical) statement. Under change of the C axis orientation in spite of the sample/load symmetry, the symmetry of solution disappears and the problem should be solved for a three-dimensional (space) statement.

The sample dimensions also affect significantly the stress–strain state. A plane stress state is realized for rather thin samples (thickness 0.5 mm and less), an axial stress component arises and increases for thicker samples. The plane strain state occurs principally in a transversally isotropic rod or tube except in its zones near ends.

The anisotropy/scale effect is displayed in Table 3. Transition from the axi-symmetrical orientation of a (0001) sample to a $\{011\ \bar{2}\}$ spatial orientation as well as the transition from a plane-stress condition (H = 0.5 mm) to a plane-strain state increases the level of arising stresses. The anisotropy of crystal essentially changes the spatial distribution pattern for stress components. For example, the tangential stresses σ_θ on a circle of a cylinder with a $\{011\ \bar{2}\}$ orientation arising in quenching is depicted in Fig. 3. Fig. 4 represents the stress component distribution along the radius of a (0001) oriented disk, 10 mm in diameter, 2.5 mm thick, for quenching (a) and heating tests (b). Calculated peak stresses for the samples tested, having the initial temperature T, are provided in Table 4. Also, Table 4 gives the time τ to reach the peak stress and the surface temperature T_f at that moment. Note, that in the water-cooled samples the peak tensile stresses are reached in 0.025–0.09 s since cooling start, before a peak radial T-difference. For the tin-heated samples, the peak stresses take place far later. Here, the peak tensile stresses occur after origination of the peak radial temperature drop, and the peak compressive stresses appears before the peak temperature drop.

Table 2
Peak values of major stresses σ_1 and time τ to reach them for water-quenched disks, diameter 10 mm, thickness 2.5 mm, heated up to 200 °C at varying λ and h

λ (W/m K)	h (W/m^2 K)	τ (s)	σ_1 (MPa)
16	30 000	0.10	241
16	14 000	0.17	176
23	14 000	0.17	147
From Table 1	From Fig. 2a	0.07	160

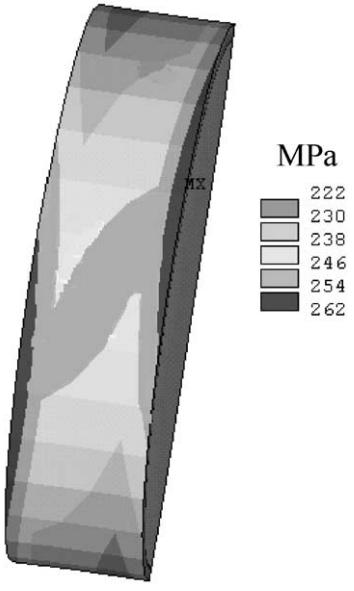

Fig. 3. Computer picture of non-uniform distribution of tangential stress σ_θ along axis and radius of cylinder $d = 10$ mm, $H = 2.5$ mm, orientation $\{011\ \bar{2}\}$ quenched in water from 200 °C after 0.08 s from the onset of cooling.

Table 3
Changes of a maximum main stress σ_1 and time τ to reach it, for samples with diameter 10 mm and height H quenched in water

Thickness of sample (mm)	Orientation	Temperature 200°C		Temperature 220°C	
		τ (s)	σ_1 (MPa)	τ (s)	σ_1 (MPa)
$H = 0.5$	(0001)	0.08	143	0.07	175
$H = 2.5$	(0001)	0.07	160	0.06	196
$H = 2.5$	$\{011\ \bar{2}\}$	0.08	177	0.08	216
$H = 5$	{0001}	0.08	167	0.08	216

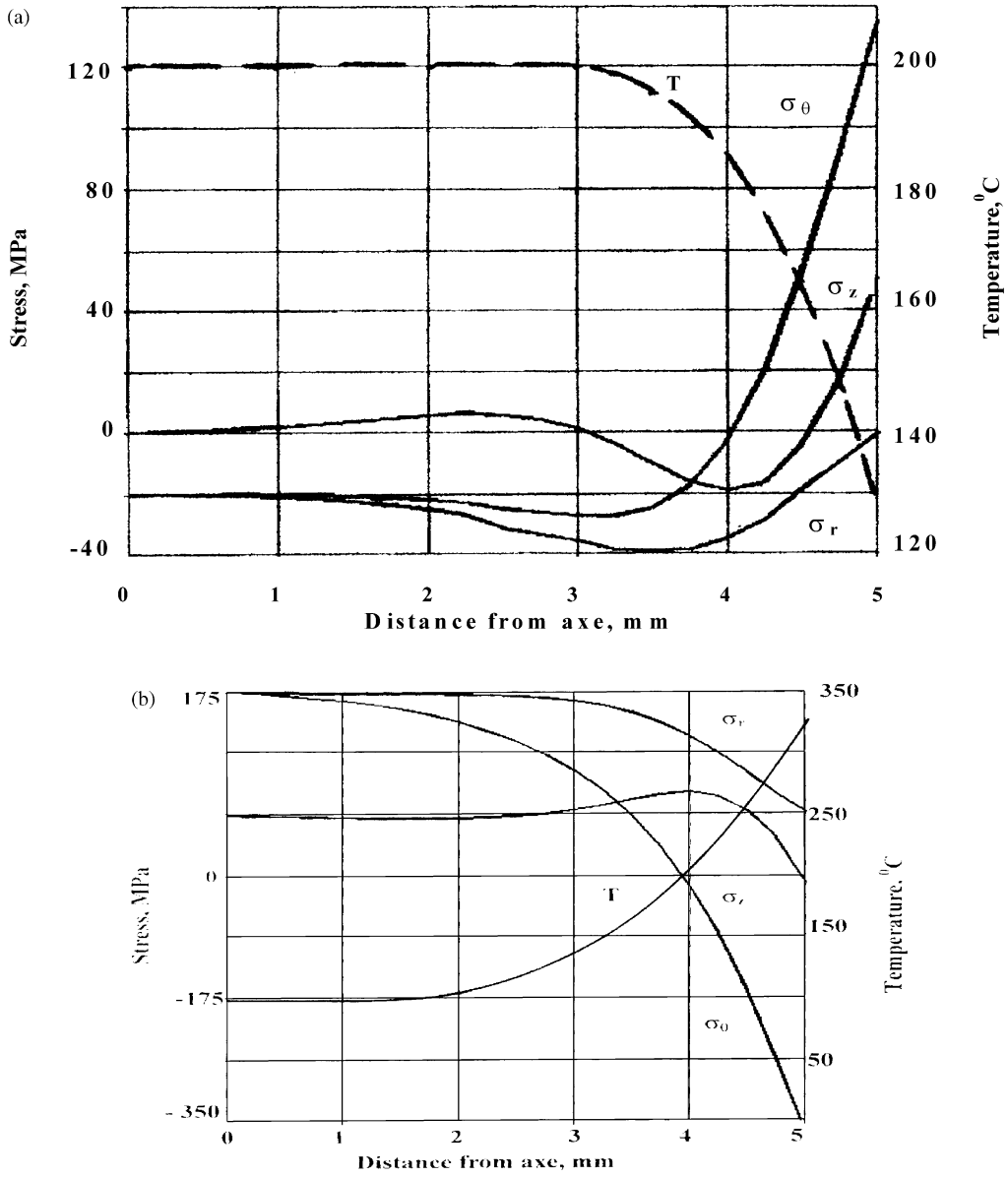

Fig. 4. Distribution of surface temperature T and stress components σ_θ, σ_r, σ_z along sample radius [$d=10$ mm, $H=2.5$ mm, orientation (0001)], quenched in water from 200 °C at the time of attainment of maximum tensile stress (a) and heated in melted tin from temperature 1000 °C at moment of attainment of maximum compression stress after 0.4 s from the onset of heating (b).

3. Results

3.1. Sample shape/orientation effect upon TSR

The TSR of sapphire is estimated in Table 4 from the level of tensile stresses (σ_z for cylinders, σ_θ for disk). These values were calculated for the mean temperature difference ΔT_m over temperature difference span ($\Delta T_{min}-\Delta T_{max}$) initiating the fracture. The number of tested specimens varied within 2–24. Dispersion of temperature difference from its mean value is about 30% for cylindrical specimens, and, as a rule, twice lower for disks. The TSR of sapphire depends significantly on the sample surface condition, orientation and shape. The stress components σ_r, σ_z, σ_θ, time τ to reach the peak stressτ and surface temperature T_f vary. The TSR of a single crystal of two different orientations (batches XV and XVI) exceeds considerably the TSR of size-similar polycrystals (batch XVII) (Table 4). The TSR of cylindrical specimens with as-grown surface (batch IR) is by 40% lower than the TSR of the specimens with polished surface (batches IV–VII) of the same crystallographic orientation. The presence of pores in the middle of rods in batch VI (1–3 μm size, maximum density 10^4 mm^2) and pores on the surface of specimens in batch VII practically did not tell on their TSR, in comparison with non-porous products (batches IV–V). In all cases the arising surface cracks in the specimens

Table 4
TSR of tested specimens

Batches	D—diameter, l, H—length, height, mm	Orientation	Number of samples	TSR				Surface temperature, T_f (°C)	Time at fracture, τ (s)
				$\Delta T_{min}-\Delta T_{max}/\Delta T_m$, °C	σ_r, MPa	σ_z, MPa	σ_θ, MPa		
B	$D=5$; $l=15$	Polycrystal	18	155–190/170			130[a]		
IR	$D=4.4$; $l=40$	(0001)	24	138–200/179	0	184	150	142	0.025
IV–V	$D=3.2$; $l=40$	(0001)	14	158–235/210					
VI	$D=3.2$; $l=40$	(0001)	7	184–261/229	0	258	212		
VII	$D=3.2$; $l=40$	(0001)	7	221–235/229	0	258	212		
IX	$D=10$; $H=2,5$	{011 $\bar{2}$}	7	210–240/224	0	70	235	142	0.07
X	$D=10$; $H=2,5$	(0001)	5	180–200/180	0	59	148	130	0.07
X**	$D=10$; $H=2,5$	(0001)	2	980/980	175/0	0/–100	175/–454	47/332	0.4[1)]
					222/0	0/–40	222/–374	200/457	1.2[2)]
X 3	$D=10$; $H=2,5$	(0001)	2	280–360/320			320		
XI	$D=20$; $H=1$	(0001)	8	190–345/218	0	5	232	138	0.09
XII	$D=25$; $H=1$	{10 $\bar{2}$0}	4	180–194/188					
XIV3	$D=20$, $H=1$	{0001}	2	200–234/230	0	7	235	135	0.09
XV	$D_o=13$; $D_i=9$, $l=9$	(0001)	4	200–260/220	0	289	330	103	0.09
XVI	$D_o=13$; $D_i=9$, $l=9$	{011 $\bar{2}$}	4	200–310/230	0	348	359	138	0.06
XVII	$D_o=13$; $D_i=9$, $l=9$	Polycrystal	7	140–215/180	0	0	154	119	0.06
XIII**	$D=20$; $H=1$	(0001)	4	520–700/595	121/0	0	121/–418	23/277	1.0[1)]
					169/0	0	169/–379	113/344	3.0[2)]
XVIII**	$D=20$; $H=1$	{10 $\bar{2}$0}	2	500–500					
XIX**	$D=30$; $H=1$	{10 $\bar{2}$0}	2	430–500/480					

Note: (D_o)—outside and (D_i) inside diameter of tubes; B—The data of paper in Ref. 1.

[a] Approximate estimate. The specimens of all batches are tested by quenching method except those of batches X**, XIII**, XVIII**, XIX** tested in melted tin. (1) At the peak compressive stress moment; (2) At the peak tensile stress moment. Numerator: center, denominator: edge. X3 and XIV3—the specimens tested by quenching after appropriate processing in melted tin and in air.

do not result to total fragmentation, saving 30% of the initial strength, as in tests of polycrystal.[1]

For as-grown samples, the cracking occur on the planes {11 $\bar{2}$0} in most cases, and less often at a 60° angle to the cylinder axis (Fig. 5a). For as-ground samples the cracking takes place mainly on the inclined planes, with separate segments of propagation on the prism planes (Fig. 5b). The TSR of the disks with (0001)-oriented end surface, (batch X) is lower than the TSR of specimens (batch IX,) whose basal plane is inclined at a 57° angle to the cylinder axis. The fracture of cylinders with the end face plane oriented as {011 $\bar{2}$} happens in main on the rhombohedral planes {02 $\bar{2}$1}. The cylinders with the basal end face plane fail on the prism planes {10 $\bar{2}$0} and {$\bar{1}$100}.

The cracks in the disks of batch XI propagate mainly on the planes of easiest cleavage {11 $\bar{2}$0} (Fig. 6a), when the cracks, originating at points of maximum circular stress (Fig. 3) in the disks of batch XII go on the rhombohedron plane {10 $\bar{1}$1} and then propagate on twisting path (Fig. 6b) with an irrational surface of fracture. The specimens fail to separate fragments in both cases. It is significant that in the plane-stress state the specimens of batches IX and X, having the component of stress σ_z, fail partially (Fig. 6c,d) with different TSR level, in contrast to a full fragmentation of the

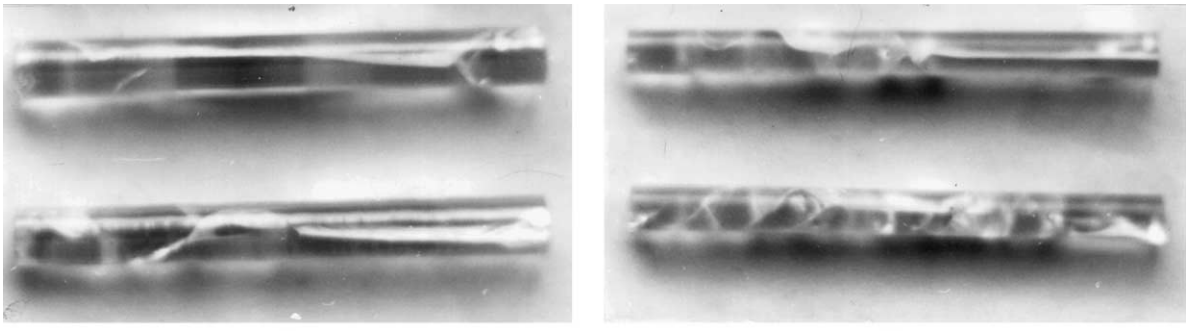

(a) (b)

Fig. 5. Fracture mode of cylindrical specimens with as grown (a) and polished surfaces (b) tested by quenching method.

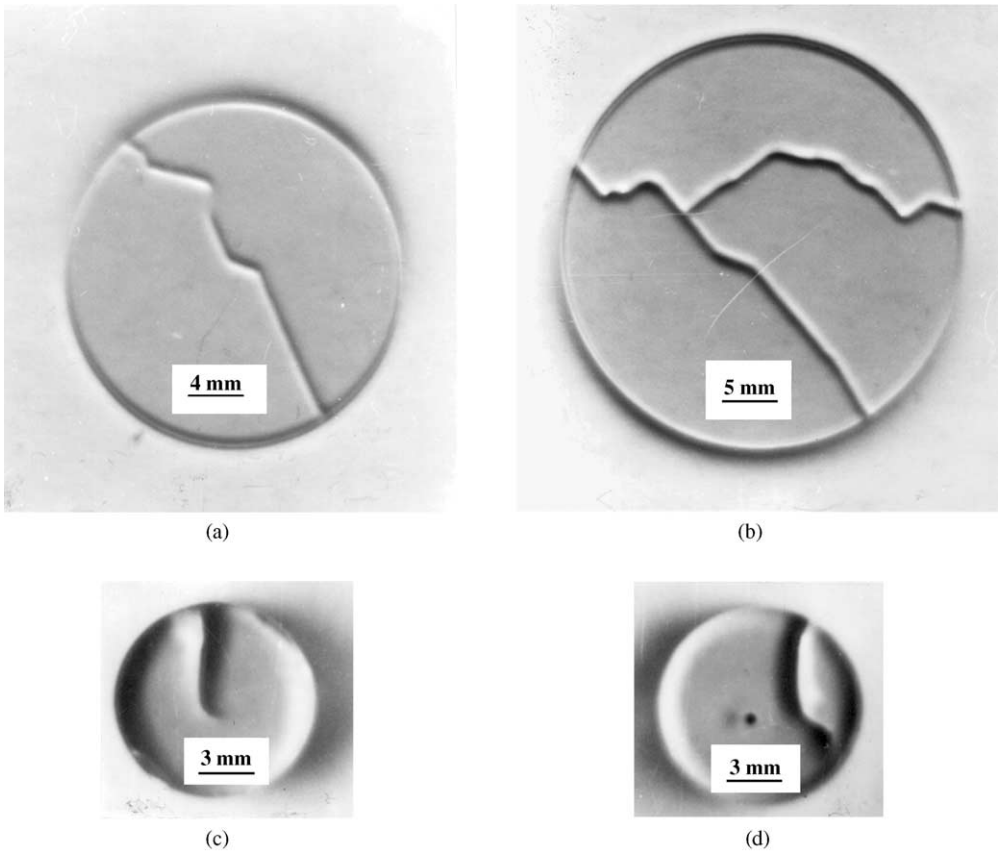

Fig. 6. Sapphire thin disks ($h = 1$ mm) with orientation {0001} (a) and {11 $\bar{2}$0} (c) and thick disks ($H = 2.5$ mm) with orientation {0001} (b) and {011 $\bar{2}$} (d) tested by quenching method.

specimens of batches XI and XII. A lower level TSR (batch X) in comparison with batch IX is due to an easier cleavage on {$\bar{1}$010} plane (Table 4).

Heat testing of thin disks of batch XIII gives rise to cracking while the same test does not cause the cracks in thick disks of batch X** at closely approximating values of σ_θ. Under tin heating, maximum compression stresses are reached first, and maximum tensile stresses come after the peak in radial temperature difference has been reached. In the initial heating period, the compressive stresses considerably exceed the tensile ones. With further heating, the difference between the compressive and tensile stress decreases. Batch XIII disks fail first on the planes {$\bar{1}$010} (Fig. 7a,b). Then, the crack moves by 90° otherwise: that is to say on the planes {10 $\bar{2}$0} (Fig. 7a). A rectilinear propagation of the crack in the {11 $\bar{2}$0} oriented disks is observed only on the initial leg of its origin on the plane {$\bar{1}$010} being across {11 $\bar{2}$0} plane. Then the crack smoothly departs from the initial direction towards the disk rim (Fig. 7c,d). It is peculiar, that the thin disks tested by heating are damaged only partially unlike full fragmentation of the disks quenched in water. The systems of twins on the planes {0001}, {$\bar{1}$012} and {11 $\bar{2}$1} observed under small magnification in the surface layers of disks of both orientations, as a system of fine (10–20 μm) sheets, extending up to 5000 μm, as a rule, arise before the cracks. Twinning occurs on the planes {$\bar{1}$012} and {11 $\bar{2}$1} in the disks of batch XIII with the orientation {0001}. The plane {$\bar{1}$012} is located at a small angle to the plane {0001}, therefore the twins when observed in a microscope, create an interference pattern with the interference band width $d \approx 800$–1000 μm (Fig. 8b). The plane {11 $\bar{2}$1} in the disk of batch XVIII is at a large angle to the plane {11 $\bar{2}$0}, and the twins are almost perpendicular to the surface of the disk owing to the interference band width is insignificant: $d \approx 30$–60 μm (Fig. 8a). In most cases cracks arise in a specimen after twinning. The combined arrangement of the twins and the cracks is depicted in Fig. 9. Only in one case a part of a crack on {10 $\bar{2}$0} plane is probably connected with fracture on the boundary between the twin and {11 $\bar{2}$1} plane.

The TSR level of batch X3 disks tested by quenching after 6–11 cyclic heating in melted tin up to 1000°C increases almost twice, obviously, because of intense twinning in the sample body and redistribution of stresses. Here, the fracture is characterised by skin-deep, symmetrically arranged radial cracks. (Fig. 10). Radiation cooling in air of side surface disks heated to 1000 °C (batch XIV3) practically does change their TSR.

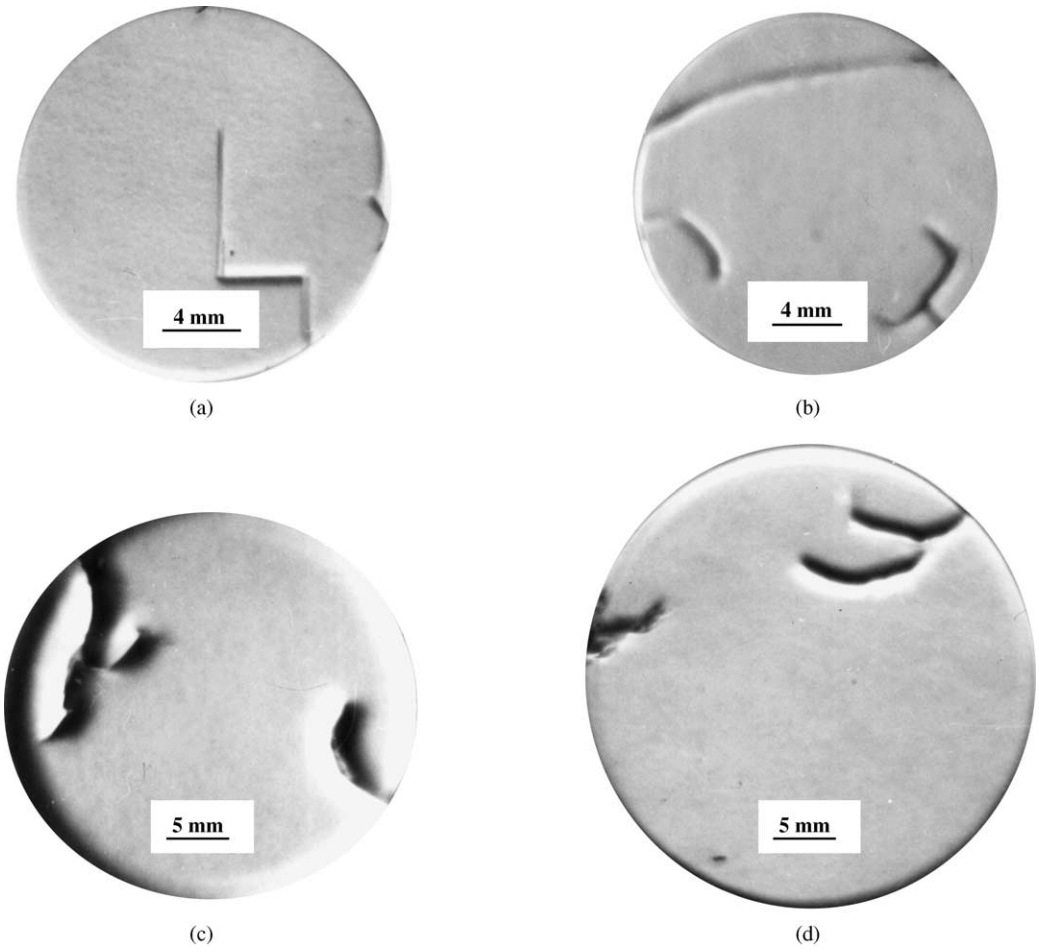

Fig. 7. Fracture mode of specimens with orientation {0001} (a, b) and {011 $\bar{2}$} (c, d) tested in melted tin at 500–600 °C.

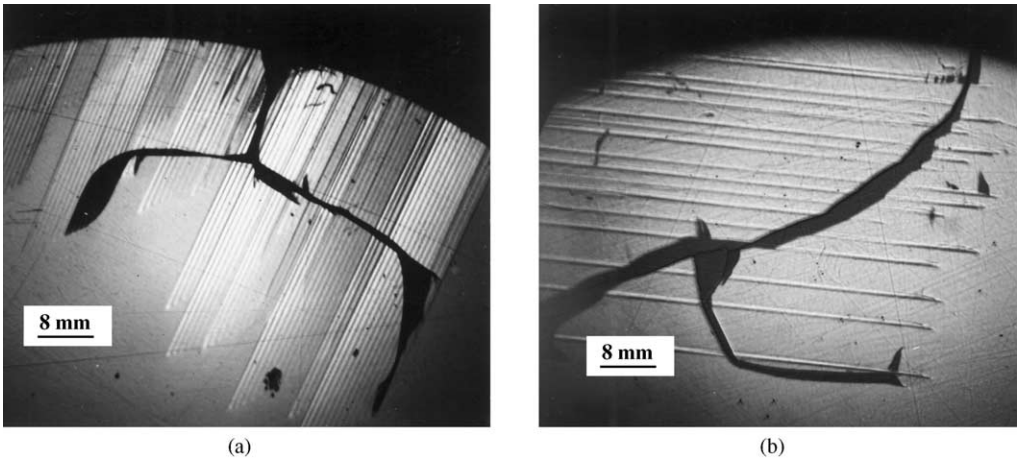

Fig. 8. Structure of twins in specimens with orientation {0001} (a) and {011 $\bar{2}$} (b) tested in melted tin at 550 °C.

3.2. Influence of thermal stresses relaxation on TSR

The heating of the lateral area of 20 mm diameter, 1 mm width disks in the induction installation II with a producing of a 150 °C temperature radial difference causes thermal-elastic tangential compression stresses on the surface. These stresses relaxation at temperatures more than 1200 °C and exposure is equal to or greater than 15 min results in tensile stresses in the surface layers exceeding the tensile strength, and then the disks fail under cooling. (Table 5). In most cases, one of cracks intersects the whole sample diametrical cross section. At the same time, the heating up to 1200 °C and a shorter exposure for 3–5 min or heating to 1000–1100 °C and a

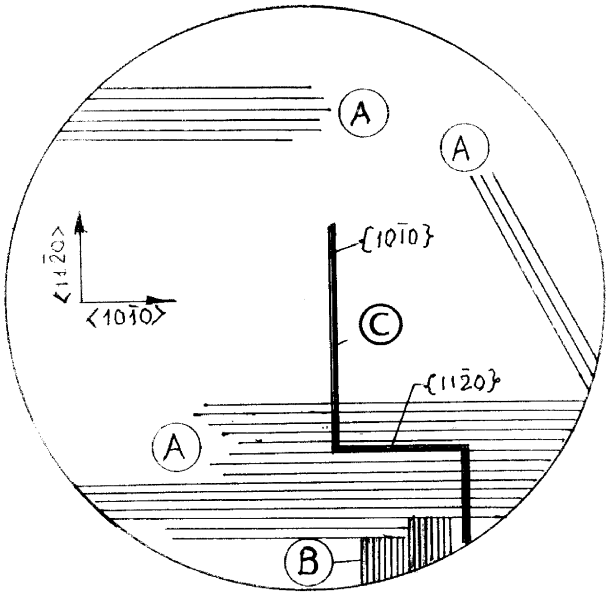

Fig. 9. Pattern of twins and cracks location in specimen with orientation {0001} after testing in melted tin at 550 °C.

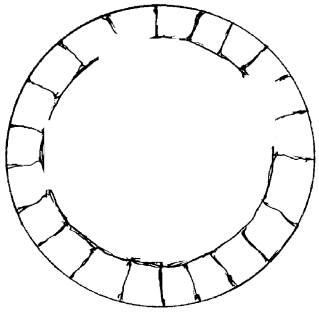

Fig. 10. Schematic of cracks pattern in specimen with orientation {0001} preliminarily cycled 8–10 times from 1000 °C in melted tin to 20 °C in air and then tested by the quenching method in water.

Table 5
Parameters inducing residual stresses in the polished sapphire disks [20 mm diameter, 1 mm thick, (0001)-end surface]

Center temperature, T_c °C	Surface temperature, T_s °C	Temperature difference, ΔT °C	Exposure, min	Sample's condition
1000	900	100	15	Unfractured
1050	900	150	15	Unfractured
1100	950	150	15	Unfractured
1200	1050	150	3	Unfractured
1200	1050	150	5	Unfractured
1200	1050	150	15	Fractured
1200	1050	150	15	Fractured
1200	1050	150	20	Fractured
1300	1150	150	10	Fractured
1350	1200	150	3	Fractured
1300	1100	200	0	Fractured[a]
1350	1150	200	0	Fractured[a]

[a] Samples are fragmented under the effect of thermal-elastic tensile stresses in the central zone of disk.

hold for 15 min do not cause fracture after cooling (Table 5). With heating up to 1200–1300 °C and a 200 °C difference, disks instantly fracture to numerous fragments due to thermal-elastic tensile stresses in their central zone.

Because both the temperature was measured in experiments only at two points only (in the centre and at the edge of the disk) and the form of the temperature field was not precisely known, respective stresses can be evaluated approximately, only. Assuming, that the temperature radial distribution follows the quadratic parabola, then the compressive stresses on the surface of the disk at the mean temperature of 1100 °C, will be 210 MPa, twice higher than the tensile stresses in the centre of the disk. After relaxation, the tensile stresses can be close to 210 MPa in the circumferential zone of the disk, thus being sufficient to induce fracture. The ratio of single-axis tensile strength to four point flexure strength of sapphire at 800 °C makes up 1/2.[5] The tensile strength of polycrystals corresponds approximately to 1/3–1/2 of the three-point bending strength.[21] Proceeding from the above and Table 7 data, where three-point flexure strength at temperature 1100 °C is 370 MPa, the tensile strength should lie in the range 123–185 MPa.

In unfractured cooled disks (Table 5), the level of residual tensile stresses does not reach the ultimate strength, but is sufficient to lower the TSR by 25–30% in the quench test. The capability for stresses to relax in sapphire at temperatures up to 1000 °C is traceable through an X-line width variation (Fig. 11).

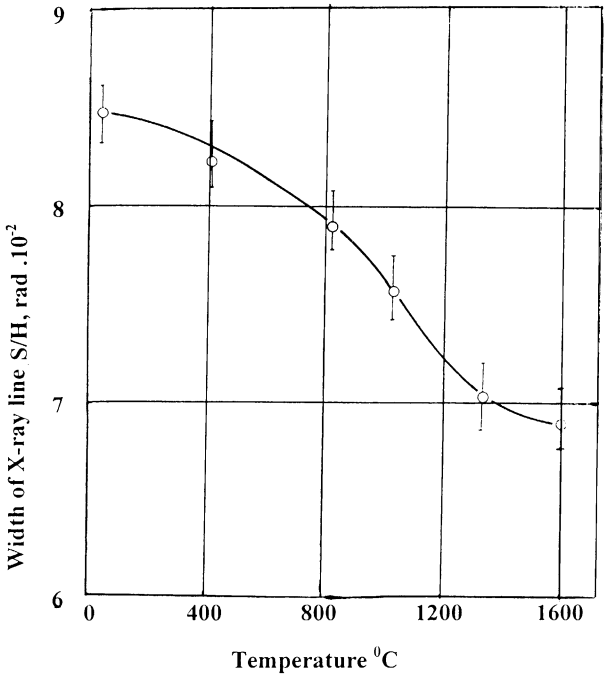

Fig. 11. Change of integral width of X-ray line (1120) as function of temperature.

Formation of thermal-elastic compression stresses on the surface of heated-cooled samples of sapphire due to relaxation is capable to increase the strength and TSR. A strengthening becomes possible at temperatures higher than the brittle–plastic transition point. A slow heating of cylindrical specimens (10 mm in diameter) up to 1600 °C in the induction installation I (without temperature difference) followed by the cooling in air of their lateral area produce surface compression stresses at a 200 MPa level. The TSR of these specimens tested by quenching increases on the average, by 35%. Sapphire, as well as polycrystal Al_2O_3,[22] should in contrast to metals, be quenched only at rather low values of the Biot's number: $ah/\lambda = 0.3$–0.8. At higher values of the Biot's number, the rate of relaxation of thermal-elastic stresses turns out to be less than the rate of their increment that leads to cracking of the body. Depending on the level and distribution of residual stresses after relaxation, the TSR of samples can essentially vary. Generation of compressive stresses on the sample surface increases the TSR and at the same time appearance of tensile surface stresses reduces the level of TSR. In greater detail the influence of residual stresses on the TSR and the behaviour of fracture with change in the thermal loading type is considered on the example of zirconium carbide.[23]

Table 6
Influences of thermal-mechanical processing on the strength of cylindrical specimens 2 mm in diameter with as grown surface. Initial three point bending strength 350 MPa

Temperature (°C)	Number of samples	Three point bending strength (MPa)
1500	3	430, 480, 495
1600	3	550, 620, 670
1700	3	890, 915, 990
1900	3	735, 800, 890
2000	5	602, 630, 770, 790, 1220

3.3. Influence of thermal-mechanical processing on TSR

The use of thermal-mechanical process is well known method[24,25] to strengthen brittle ceramic compounds. The essence of the method consists in relaxation of local stresses nearby concentrators of stresses during static or active loading at a low rate under stresses close to the yield point of a material. In the present work the chosen processing method is similar to the thermal-mechanical strengthening method The method lies in a creation of thermal stresses, sufficient to relax local stresses on defects during thermal loading.

Required thermal stresses were produced by rapid insertion of a sample from the cold chamber into the upper chamber, heated up to high temperatures in the induction installation I. Thermal-elastic compression stresses on the surface of a cylindrical sample (2 mm in diameter) reach 25–50 MPa in a fraction of a second at heating temperatures of 1500–2000 °C. After 30–60 s exposure in the furnace, the samples are cooled with a temperature rate 1–5 °C. The stresses approximately evaluated for the value of the reduced emissivity $\varepsilon_r = 0.6$ turn out sufficient to start motion of dislocations and reduce the stress concentrators on defects through relaxation. As shown in Ref. 26, the stresses found for start of dislocations near the indentor print in ionic crystals at the temperature of 0.22 T_m, are about 7 MPa, that is several times lower than the stresses produced at this temperature level in thermal-mechanical processing. The strength of thermal-mechanically treated specimens after cooling increases up to 3 times (Table 6). Unlike quenching, the thermal-mechanical strengthening of specimens after consequent isothermal heating cycles is not lost.

The capability of thermal-mechanical strengthening for sapphire is confirmed by experiments with mechanical loading upon specimens with intended cracks applied to the surface by indentation.[27] The strengthening

Table 7
Strength σ of sapphire specimens under three point flexure and tension and variation coefficient W

Batch	Number of specimens	Temperature (°C)	Dimesions (mm)	Orientation of axis	Loading mode	σ_{min}–σ_{max}/σ_m (MPa)	$W = S/\sigma_m$ (%)
I	7	20	$D_o = 4.4$; $l = 40$	(0001)	Three-point flexure	420–570/490	
IV	7	20	$D_o = 3.2$; $l = 40$	(0001)	Three-point flexure	590–840/750	
XV	50	20	$D_o = 13$; $D_i = 9$, $l = 9$	(0001)	Tension	81–801/453	29
XVI	45	20	$D_o = 13$; $D_i = 9$, $l = 9$	{01 $\bar{2}$1}	Tension	241–780/533	35
XVII	47	20	$D_o = 13$; $D_i = 9$, $l = 9$	Polycrystal	Tension	121–286/177	21
B	18	20	5×5×10	Polycrystal	Three-point flexure	193–478/336	
XX[a]	3	20	3×3×17	(0001)	Three-point flexure	800–1330/994	
XX[a]	3	600	3×3×17	(0001)	Three-point flexure	316–600/485	
XX[a]	3	1100	3×3×17	(0001)	Three-point flexure	233–632/370	
XX[a]	3	1650	3×3×17	(0001)	Three-point flexure	269–372/314	

$W = S/\sigma_m$, where S—is a mean root square deviation of strength, σ_m is a mean arithmetic value of strength.

[a] Specimens were ground and then polished up to Ra = 0.32 μm, edges chamfered. Face plane (0001). Lateral tensile face plane {10 $\bar{2}$0}. B—data of paper Ref. 1.

was conducted at 1110–1160 °C slightly exceeding the point of brittle-plastic transition, but under higher stresses of 0.5–0.95 of the ultimate strength at 20 °C. These experiments (authors state as preliminary) and the thermal-mechanical processing parameters used can not be considered as optimal.

4. Discussion

The heat-induced fracture of sapphire essentially differs from established regularities of thermal fracture of ceramic materials owing to sapphire strain by twinning at rather low temperatures: 0.2 $T_{m.}$. This feature predetermines distinctions in the character of cracking with change of the thermal loading type upon sapphire and polycrystalline oxide/nonoxide compounds, incapable of plastic deformation up to temperatures of 0.4–0.6 T_m. The sapphire anisotropy of properties aggravates the observable gap in the TSR of sapphire and polycrystal.

The cracks originating on the surface of quench-tested quasi-isotropic polycrystals stop in the compressed central zone; full fragmentation is excluded. At the same time, the heating tests lead, as a rule, to full fragmentation of the polycrystals due to tensile stresses in the central zone, despite the presence of compression stresses in the peripheral zone (Fig. 12). It is established, that partial or full fracture of the brittle isotropic bodies is determined by a non-uniformity of the stress field characterised by an N parameter.[28,29] This parameter takes into account not only the ratio between the tensile and compression zones, but also the stress distribution of stresses in these zones. At $N \leqslant 0{,}1$, that is under the stress condition with rather large zones of compression, the started crack stops, and full fragmentation may be reached under load several times higher than the load to start the crack.[30,31] Full fracture of a body under uniaxial compression also proceeds with increasing load with a certain interaction of growing cracks.[32,33]

Sapphire unlike polycrystals fails in a different way with change of thermal loading. Under heating test, only surface cracks occur in sapphire disks (Figs. 7–9) at 500–600 °C, while in quench test, the disks are fragmented completely. The feature of fracture in the heating test resides in the capability of twinning in sapphire within low temperatures and stresses. For example, the critical resolved stress of twinning on the rhombohedral planes $\{\bar{1}012\}$ reaches 230 MPa at 350 °C and decreases down to 30 MPa at 600 °C,[34] that is 13 times below the arising thermal stresses. Relaxation of thermal compressive stresses by twinning, and formation of residual tensile stresses after cooling, close in their absolute level to the initial thermal-elastic compression stress (Table 4), appear to be sufficient for surface cracking. At the same time, thermal-elastic tensile stresses in the central zone of the disk as high as 120–170 MPa are below the single-axis tensile strength at the same temperature[5] and not sufficient to cause cracking. The plastic deformation by sliding is especially impossible because, even at 800 °C, the critical stresses on the basal, prismatic and pyramidal planes are about 900 MPa.[34] No twins in the central zone of the disk are explained by unfavorable conditions for them to be born in the tensile stress zone, as proved in Ref. 5. A smooth departure of the crack from its initial direction to the rim of the disk (Fig. 8) is caused by a braking influence of compression stresses in the central zone.

The disks tested by quenching fail to fragments in contrast to the surface fracture of the disks tested by heating. The tensile stresses, arising on the surface, turn out sufficient (Table 4) for cracking, but twinning and stress relaxation at test temperatures 200–250 °C is sharply reduced. The passing of the crack through the cross-section of the disk under cooling (Fig. 6), seems to be connected with an anisotropy of the singlecrystal fracture toughness. Various methods of measurement[35,36] including our own one of an indentation technique give the fracture toughness value K_{1c} or the specific fracture energy $\gamma = K_{1c}^2 (1-\nu^2)/2E$, depending on the orientation, from 2 to 4.5 MPa $m^{1/2}$ or 6–22 J/m^2, accordingly. The highest values relate to the basal plane (0001) and the lowest ones to the planes (1012), (1014). The fracture toughness of cold-hardened sapphire specimens, having residual surface stresses increases by 20–50%.[36] The specific fracture energy of polycrystalline Al_2O_3 varies non-monotonously with change of a grain size from 20 to 100 J/m^2.[21] Generally, a resistance to the crack propagation in Al_2O_3, as well as in other polycrystals, is noticeably higher than in the monocrystal due to an additional resistance of the boundaries of variously oriented grains. Owing to a reduced fracture toughness of the monocrystal, a crack beginning its motion in the tensile zone, overcomes the compression zone along more favourably oriented (least energy consuming) planes. The TSR, as well as the strength in a selected load mode, depends on the orientation of the specimen. The ratio between the levels of TSR of the

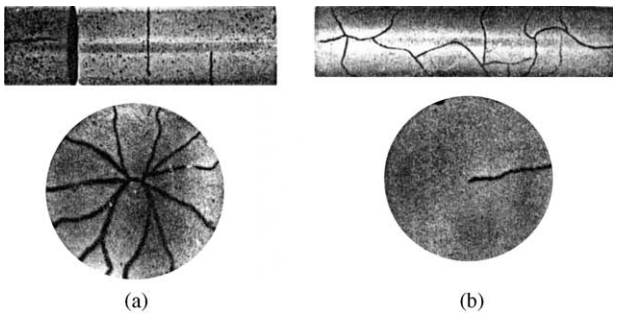

Fig. 12. Fracture mode of disks 25 mm in diameter and cylinders 12 mm in diameter from polycrystal ZrC tested by heating in melted tin (a) and by quenching method in water (b).

cylindrical specimens of batches XV and XVII is similar to the ratio between tensile strength of these batches (Table 7). The strength of specimens under uniaxial compression at 20 °C is 5–7 times greater than the uniaxial tensile strength.[32] The four-point flexure strength of the prismatic specimens having the plane $\{11\ \bar{2}0\}$ and the direction [0001] parallel to the tension axis, is almost twice the strength of the specimens with the same plane and the direction along $[10\ \bar{1}0]$ axis.[5] The observable anisotropy of strength and TSR of sapphire results from the crystallographic function of the fracture energy γ. The cylinders of batch XVI fail under quenching test mainly on the rhombohedral planes $\{02\ \bar{2}1\}$. The cylinders (batch XV) with the basal face surface fail on the prism planes $\{10\ \bar{2}0\}$.

Fracture pattern examination of tested sapphire (batch XX) (Table 7) has shown, that a macroscopic fracture happens in the basal plane, though local fractures develop on the cleavage planes such as $\{10\ \bar{1}1\}$, less often on irrational surfaces and boundaries of blocks. The fracture origins are, first of all, sample surface defects appearing during growth and machining. The bending load–displacement diagrams for samples of batch XX are nearly linear up to 1100 °C. Polycrystalline specimens fail mainly on the grain boundaries, only separate large grains fail by cleavage, and the level of their strength is significantly lower than that of monocrystal.

Depending on selected growth modes of singlecrystal by Stepanov's method, the strength of as-grown cylindrical specimens varies from 300 to 1100 MPa. Machining of high-strength samples, as a rule, reduces their strength. Grinding and polishing of as-grown samples (batch I) with a reduced strength provides strengthening due to reduction of defects and inducing of compressive stresses in the surface layers (batch IV) (Table 7). The surface finish has the same influence on the TSR (Table 4). Indeed, the X-raying[37] showed that 135–170 MPa compression stresses are produced in the surface layers equaled to or greater than 15 μm deep, after diamond processing of sapphire.

A basic problem of the fracture mechanics for thermally loaded bodies consists in determination of their fracture conditions. The tension-induced propagation of a crack in an elastic–brittle body is possible with reaching the critical stress intensity factor K_{1c}. The subsequent cracking and fracture type are defined by non uniformity of thermal stress field.[28,29] Materials akin to sapphire capable to undergo anisotropic plastic deformation under heating are fractured in a more complex way. It becomes necessary to take into account stress relaxation due to twinning and redistribution of stresses through the whole body at rather low temperature. The characteristic pattern of fracture of disks (Fig. 10) is associated with redistribution of thermal-elastic stresses and with strengthening of surface layers as a consequence of twinning under cyclic heating.

The computational evaluations of relaxation processes in thermal stress fields are difficult[38] or rather rough.[39] More reliably the stress relaxation could be assessed experimentally by X-ray $\sin^2 \psi$ method or by method of opening a cut in stressed bodies.[23]

5. Conclusion

The fracture behaviour of sapphire in comparison with this of polycrystalline materials under thermal loading is governed by two phenomenon: the capability of deformation by twinning at rather low temperatures of test 200–300 °C and by the fracture toughness anisotropy. The observable behaviour of cracking and TSR with change of sample crystallographic orientation and thermal loading type is explained on the basis of force fracture mechanics. The current models of TSR[40,41] using energetic principles of fracture, neglect a physical difference in the cracking behaviour in the tension and compression fields and are not able to adequately describe the cracking behaviour in non uniform heat stress fields. The series of experiments performed on thermal-mechanical processing of sapphire, leading to formation of thermal stresses, have established the capability to essentially increase the sapphire strength due to local stress relaxation and lower stress concentration on the crystal defects.

Acknowledgements

The authors appreciate the assistance of V.I Korolev for supplying various forms of specimens and of V.A. Popenko, who performed the X-ray orientation of the specimens. This Research is supported by the Russian Fund of Basic Research (Grant No. 2002–01).

References

1. Davidge, R. W. and Tappin, G., Thermal shock and fracture in ceramics. *Trans. Brit. Ceram. Soc.*, 1967, **66**, 405–422.
2. Gupta, T. K., Strength degradation and crack propagation in thermally shocked Al_2O_3. *J. Am. Ceram. Soc.*, 1988, **55**(N5), 249–253.
3. Glandus, C. P. and Boch, P., Influence of the size factor on the thermal shock resistancå of ceramic samples. *Int. J. Thermphys.*, 1981, **2**, 89–100.
4. Nicolaev, Y. V., Vasilchenko, A. V. and Lapochkin, N. V., High-voltage metal-ceramic assembly of thermîionic NPP. In *Proc. of 12th Symposium on Space Nuclear Power and Propulsion*, ed. M. S. EL-Genk. AIP Conference Proc. N 324, Vol. 1. American Institute of Physics, New York, pp. 289–294.
5. Schmid, F. and Harris, D. C., Effect of crystal orientation and temperature on the strength of Sapphire. *J. Am. Ceram. Soc.*, 1998, **81**, 885–937.
6. Stepanov, A. V., New method of manufacture of products of various profiles immediately from melt. *Zhurnal technicheskoy fiziki*, 1959, **29**, 381–393 (in Russian).

7. Lanin, G., Methods of testing for heat resistance (review). *Industrial Laboratory*, **64** (1998), (3), 168–192 (translated from Russian, *Zavodskaya Laboratoriya*, 1998, **64**(3), 31–46.
8. Lanin, A. G., Âorunov, V. V., Egorov, V. S., et al., Heat resistance of materials and structural elements. In *Collection of Research Papers*, Issue 5. Naukova Dumka, Kiev, 1969, pp. 284–293 (in Russian).
9. Lanin, A. G. and Popov, V. P., Thermal shock resistance of materials by induction heating. In *Proceed. of International Symposium on Thermal Stresses and Related Topics*. Hamamatsu, Japan, 1995, pp. 87–89.
10. Lanin, A. G. and Tkachev, A. L., Numerical method of thermal shock resistance estimation by quenching of samples in water. *J. Mater. Sci.*, 2000, **35**, 2553–2559.
11. Lanin, A. G., Thermal shock resistance of porous SI_3N_4, ZrC, heterogenous carbides and hydrides. In *Proceedings Fracture Mechanics of Ceramics*, Vol. II. Plenum Press, 1996, pp. 523–529.
12. Borunov, V. V., Egorov, V. S. and Lanin, A. G., Thermal stresses in cylinder during thermal stress resistance tests in transient heat transfer conditions. *Ingenerno Phys J.*, 1968, **24**(4), 684–688 (in Russian).
13. Gao, T., Nishikwa, T., Hibi, M. and Takatsu, M., Temperature dependence of so-called heat transfer coefficient under thermal shock test. *J. Ceram. Soc. Japan*, 1993, **101**(N7), 788–792.
14. Awaji, H., Takahashi, T., Yamamoto, N. and Nishikawa, T., Analysis of temperature/stress distribution in thermal shocked ceramic disks in relation to temperature-dependant properties. *J. Ceram. Soc. Japan*, 1998, **106**(N4), 358–362.
15. Boley, B. A. and Weiner, J. C., *Theory of Thermal Stresses*. J. Wiley and Sons, New York, 1960.
16. Hasselman, D. P. H., Thermal shock by radiation heating. *J. Am. Ceram. Soc.*, 1963, **46**, 229–234.
17. Kondratev, G. M., *Thermal Measurements*. Mashgiz, 1957 (in Russian).
18. Anon., *ANSYS Programmer's Manual*, Revision 5.5. ANSYS Inc., 1999.
19. Antonov, I. I., Bacholdin, C. I., Vandakurov, I. Y. U., Galaktionov, E. V. and Tropp, E. A., Influence of anisotropy of thermal-phyisical and elastic properties on thermal stresses in profile monocrystal of sapphire and NbLi. *Izvestya A.N. SSSR, Series Physical*, 1983, **47**, 286–294 (in Russian).
20. Miyazaki, N., Uchida, H., Tsukada, T. and Fukuda, T., Quantitative assessment for cracking in oxide bulk single-crystals during Czochralski growth—development of a computer-program for thermal-stress analysis. *J. Crystal Growth*, 1996, **162**(1–2), 83–88.
21. Barinov, S. M. and Shevchenko, V. Ia, *Strength of Engineering Ceramics*. Nauka, Moscow, 1996 (in Russian).
22. Gebauer, J., Krohn, D. A. and Hasselman, D. P. H., Thermal-stress fracture of a thermal-mechanical strengthened aluminosilicate ceramic. *J. Am. Ceram. Soc.*, 1972, **55**, 198–201.
23. Lanin, A. G. and Deryavko, I. I., Influence of residual stresses on thermal stress resistance of refractory ceramic. *J. Eur. Ceram. Soc.*, 2000, **20**, 209–213.
24. Lanin, A. G., Erin, O. N. and Turchin, V. N., Methods of strengthening of refractory ceramic materials. In *Proceedings of World Ceramic Congress, Ceramics Today-Tomorrow's Ceramics*, Italy. Elsevier Science, 1991, pp. 1581–1590.
25. Lanin, A. G. and Turchin, V. N. *et al.*, Influence of program strengthening on ZrC mechanical properties. *Physika Chimiya Obrabotki Materialov*, 1982, **N2**, 88–92 (in Russian).
26. Lanin, A. G., Turchin, V. N. and Kovalev, D. U., Relaxation of local stresses in ZrC surfaces. *Metallofizika*, 1991, **13**(N4), 120–128 (in Russian).
27. Kim, H. and Roberts, S., Brittle-ductile transition and dislocation mobility in sapphire. *J. Am. Ceram. Soc.*, 1994, **77**, 3099–3104.
28. Lanin, A. G., Popov, V. P. and Egorov, V. S., Fracture of the cylindrical bodies from brittle materials under thermal loading. *Problemy prochnosty*, 1973, **N3**, 56–60 (in Russian).
29. Egorov, V. S., Lanin, A. G. and Fedik, I. I., Fracture of thermally loaded disks of materials in elastic-brittle state. In *Strength of Materials*. Plenum Publishing, New York, 1981, pp. 183–189 (translation from Russian in *Problemy Prochnosty*).
30. Lanin, A. G., Thermal shock resistance and fracture of ceramic materials. In collection *Thermal Shock and Thermal Fatique Behaviour of Advanced Ceramics*, ed. G. A. Schneider and G. Petzow. Series E: Applied Sciences, Vol. 241. Kluwer Academic, Dordrecht, pp. 317–330.
31. Lanin, A. G. and Ågîrîv, V. S., Fracture kinetics of thermally loaded bodies in elastic-brittle state and criterion of thermal stress resistance. In *Fracture mechanics of ceramic 13*, eds. R.C. Brandt, D. Munz. Kluwer Academic/Plenum Publishers, 2002, Vol. 13. pp. 395–411.
32. Lanin, A. G., Bochkov, N. A. and Egorov, V. S., Brittle fracture of materials in compression. In *Strength of Materials*. Plenum Publishing, New York, 1986, pp. 1274–1278 (translation from Russian in *Problemy Prochnosty* 1985, N9, 75–80).
33. Ashby, M. F. and Hallam, S. D., The failure of brittle solids containing small cracks under compressive stress state. *Acta Metall.*, 1986, **N3**, 497–510.
34. Scott, W. D. and Orr, K. K., Rhombohedral twinning in alumina. *J. Am. Ceram. Soc.*, 1983, **66**, 27–32.
35. Wiederhorn, S. M., Fracture of sapphire. *J. Am. Ceram. Soc.*, 1969, **52**, 485–491.
36. Deruygin, U. V. (Ed.), *Sapphire is in Jewellery Commercial Production*. Machinostroenie, Lenigrad, 1984 (in Russian).
37. Lange, F. F., James, M. R. and Green, D. J., Determination of residual surface stresses caused by grinding in polycrystalline Al_2O_3. *J. Am. Ceram. Soc.*, 1983, **64**, 504–511.
38. Dauknis, V. I., Kazakayvichus, K. A. and Pranzkayvichus, G. *et al.*, *Investigation of Thermal Stress Resistance of Refractory Ceramics*. Mintas, Vilnus, 1971 (in Russian).
39. Buessem, W. R. and Gruver, R. M., Computation of residual stresses in quenched Al_2O_3. *J. Am. Ceram. Soc.*, 1972, **55**, 41–44.
40. Hasselman, D. P. H., Unified theory of thermal shock fracture initiation and crack propagation in brittle ceramics. *J. Am. Ceram. Soc.*, 1969, **52**, 600–604.
41. Bahr, H. A., Bahr, U, Balke, H. et al., Multiple crack propagation under thermal load. In *Proceedings Thermal Shock and Thermal Fatigue Behaviour of Advanced Ceramics*, ed. G. A Schneider and G. Petzow. Series E: Applied Science, Vol. 241. Kluver Academic, 1992, pp. 143–153.